(1982); T. P. Stossel, *ibid.*, p. 275; G. F. Oster and G. M. Odell, *Physica D* **12**, 333 (1984).
7. C. Pasternak and E. L. Elson, *J. Cell Biol.* **100**, 860 (1985).
8. J. M. Michison and M. M. Swann, *J. Exp. Biol.* **32**, 743 (1955); Y. Hiramoto, *Exp. Cell Res.* **32**, 59 (1963).
9. T. E. Schroeder, *Proc. Natl. Acad. Sci. U.S.A.* **70**, 1688 (1973); K. Fujiwara and T. E. Pollard, *J. Cell Biol.* **71**, 848 (1976).
10. S. Yumura and Y. Fukui, *Nature (London)* **314**, 194 (1985).
11. D. E. Koppel, J. M. Oliver, R. D. Berlin, *J. Cell Biol.* **93**, 950 (1982).
12. R. Rappaport, *Int. Rev. Cytol.* **105**, 245 (1986).
13. L. Wolpert, *ibid.* **10**, 163 (1960).
14. J. G. White and G. G. Borisy, *J. Theor. Biol.* **101**, 289 (1983).
15. J. G. White, *BioEssays* **2**, 267 (1985).
16. T. E. Schroeder, *J. Cell Biol.* **53**, 419 (1972).
17. The migratory behavior of animal cells, including leukocytes and fibroblasts, is described by J. P. Trinkaus [*Cells into Organs* (Prentice-Hall, Englewood Cliffs, NJ, 1984), chaps. 7 and 11)]; and by J. M. Lackie [*Cell Movement and Cell Behaviour* (Allen and Unwin, Winchester, MA, 1986), chap. 6].
18. S. E. Malawista and A. de Boisfleury Chevance, *J. Cell Biol.* **95**, 960 (1982).
19. J. V. Small and G. Rinnerthaler, *Exp. Biol. Med.* **10**, 54 (1985); A.-S. Hoglund, R. Karlsson, E. Arro, B.-A. Fredricksson, U. Lindberg, *J. Muscle Res. Cell Motil.* **1**, 127 (1980); K. Burridge, *Cancer Rev.* **4**, 18 (1986).
20. W. H. Lewis, *Bull. Johns Hopkins Hosp.* **49**, 29 (1931).
21. W. S. Haston and J. M. Shields, *J. Cell Sci.* **68**, 227 (1984).
22. W. S. Haston, *ibid.*, **88**, 495 (1987).
23. A. De Lozanne and J. A. Spudich, *Science* **236**, 1086 (1987); D. A. Knecht and W. F. Loomis, *ibid.*, p. 1081.
24. L. Y. W. Bourguignon and G. J. Bourguignon, *Int. Rev. Cytol.* **87**, 195 (1984).
25. R. B. Taylor *et al.*, *Nature (London) New Biol.* **233**, 225 (1971).
26. M. S. Bretscher, *Sci. Am.* **257**, 72 (December 1987); S. J. Singer and A. Kupfer, *Annu. Rev. Cell. Biol.* **2**, 337 (1986).
27. S. Kater and P. Letourneau, Eds., *Biology of the Nerve Growth Cone* (Liss, New York, 1985).
28. K. H. Pfenninger, *Trends Neurosci.* **9**, 562 (1986).
29. D. Bray and K. Chapman, *J. Neurosci.* **5**, 3204 (1985); W. A. Harris, C. E. Holt, F. Bonhoeffer, *Development* **101**, 123 (1987).
30. A. K. Harris, P. Wild, D. Stopak, *Science* **208**, 177 (1980); J. M. Vasiliev, *Biochim. Biophys. Acta* **780**, 21 (1985).
31. J. R. Couchman and D. A. Rees, *J. Cell Sci.* **39**, 149 (1979).
32. M. Abercrombie, *Proc. R. Soc. London Ser. B* **207**, 129 (1980).
33. J. P. Heath, *J. Cell Sci.* **60**, 331 (1983).
34. T. M. Svitkina, A. A. Neyfakh, A. D. Bershadsky, *ibid.* **82**, 235 (1986); Y.-L. Wang, *J. Cell Biol.* **101**, 597 (1985).
35. G. A. Dunn, in *Cell Adhesion and Motility*, A. S. Curtis and J. D. Pitts, Eds. (Cambridge Univ. Press, New York, 1980), pp. 409–423; W.-T. Chen, *J. Cell Sci.* **49**, 1 (1981).
36. A valuable introduction to earlier literature on amoeboid locomotion is given by Allen and Kamiya [R. D. Allen and N. Kamiya, Eds., *Primitive Motile Systems in Cell Biology* (Academic Press, New York, 1961)].
37. W. Stockem and H. U. Hoffman, *Acta Protozool.* **25**, 245 (1986).
38. A. Grebecki, *Protoplasma* **123**, 116 (1984).
39. ———, *Acta Protozool.* **25**, 255 (1986) (figure 10 in this reference illustrates the movement of constriction rings).
40. We thank B. Alberts, K. Burridge, and J. Pine for their criticism of this work.

Research Articles

Three-Dimensional Structure of an Oncogene Protein: Catalytic Domain of Human c-H-*ras* p21

ABRAHAM M. DE VOS, LIANG TONG, MICHAEL V. MILBURN, PEDRO M. MATIAS, JARMILA JANCARIK, SHIGERU NOGUCHI, SUSUMU NISHIMURA, KAZUNOBU MIURA, EIKO OHTSUKA, SUNG-HOU KIM*

The crystal structure at 2.7 Å resolution of the normal human c-H-*ras* oncogene protein lacking a flexible carboxyl-terminal 18 residue reveals that the protein consists of a six-stranded β sheet, four α helices, and nine connecting loops. Four loops are involved in interactions with bound guanosine diphosphate: one with the phosphates, another with the ribose, and two with the guanine base. Most of the transforming proteins (in vivo and in vitro) have single amino acid substitutions at one of a few key positions in three of these four loops plus one additional loop. The biological functions of the remaining five loops and other exposed regions are at present unknown. However, one loop corresponds to the binding site for a neutralizing monoclonal antibody and another to a putative "effector region"; mutations in the latter region do not alter guanine nucleotide binding or guanosine triphosphatase activity but they do reduce the transforming activity of activated proteins. The data provide a structural basis for understanding the known biochemical properties of normal as well as activated *ras* oncogene proteins and indicate additional regions in the molecule that may possibly participate in other cellular functions.

THE MOST COMMONLY FOUND ONCOGENES ISOLATED FROM human tumors or transformed human cell lines belong to the *ras* gene family (*1*). In the human genome there are three distinct cellular *ras* genes: c-H-*ras*, c-K-*ras*, and N-*ras*, the former two having sequence similarity (*2–5*) to the transforming principles of the Harvey and Kirsten strains of rat sarcoma viruses (*6, 7*), respectively. All proteins encoded by these genes are called p21, have a molecular weight of about 21,000 with 188 or 189 amino acid residues, and have practically identical amino acid sequences, with the exception of the carboxyl-terminal 25 residues (*8*). The difference between the normal *ras* proto-oncogenes and the activated (transforming) *ras* oncogenes is usually a single base change at one of a few critical positions, resulting in a single amino acid substitution in p21 (*9–11*).

In vivo involvement of the *ras* genes in neoplasia was recently shown by the experiment that transgenic mice bearing activated c-

A. M. de Vos, L. Tong, M. V. Milburn, P. M. Matias, J. Jancarik, and S.-H. Kim are in the Department of Chemistry and Lawrence Berkeley Laboratory, University of California, Berkeley, CA 94720. S. Noguchi and S. Nishimura are in the Biology Division, National Cancer Research Institute, Chuo-ku, Tokyo, Japan. K. Miura and E. Ohtsuka are in the Faculty of Pharmaceutical Sciences, Hokkaido University, Kita-ku, Sapporo, Japan.

*To whom all correspondence should be addressed.

H-*ras* oncogene under control of the rat elastase I regulatory element developed massive tumors in the pancreas within a few days of pancreatic differentiation, while those harboring the normal proto-oncogene did not (*12*). In addition to their role in human and animal cancer, the *ras* genes have been implicated in cell proliferation, terminal differentiation, and other essential processes, suggesting that *ras* proteins may function as signal transducers, like G proteins (*13*), at the beginning of the cascade of reactions leading to these processes.

Among the biochemical properties of p21 proteins are that they bind guanosine triphosphate (GTP) and guanosine diphosphate (GDP) (*14–17*); they hydrolyze GTP to GDP (*17–21*); activated p21 proteins often show reduced GTP hydrolysis activity (*17–21*); activated proteins with a threonine at position 59 have autokinase activity, Thr^{59} being the phosphate acceptor (*22*); palmitic acid is posttranslationally attached to Cys^{186} in all p21 proteins (*23–26*), which facilitates their association with the inner surface of the cell's plasma membrane (*23, 27, 28*); the COOH-terminal 25 residues are likely to be flexible (*29–31*), are not required for any of the known biochemical functions of the protein, and only the last four residues are essential for attachment to the cell wall and transformation (*28, 32*); and the proteins have moderate sequence similarity to the GTP-binding domain of signal transducing G proteins (*13*) and other guanine nucleotide–binding proteins such as the bacterial elongation factor, EF-Tu (*33–36*).

Knowledge of the three-dimensional structure of this *ras* protein family should be most useful to provide a basis for understanding the known biochemical functions of both normal and activated proteins. We have recently crystallized the "catalytic domain" of c-H-*ras* p21 protein (residues 1 to 171), which has GDP or GTP binding and guanosine triphosphatase (GTPase) activity, as well as the intact protein (189 residues). We have also crystallized the "catalytic domains" of two activated p21 proteins, one with valine at position 12, p21 (Val^{12}), and another with leucine at position 61, p21 (Leu^{61}), as well as the corresponding intact proteins. All of the "catalytic domain" and intact normal proteins bind GDP or GTP and hydrolyze GTP, while the activated forms show reduced or absence of GTPase activity. In this article, we report the first in a series of *ras* p21 protein structures.

Protein preparation and crystallization. Preparation procedures and crystallization conditions of p21 proteins have been described (*37*). Briefly, p21 proteins have been expressed in *Escherichia coli* harboring a plasmid that contains synthetic genes coding for the amino acid residues 1 to 171 or 1 to 189 (*38*). The proteins were purified by DEAE Sephacel and Sephadex G-75 column chromatography to more than 95 percent purity by essentially the same procedure as that reported (*18*). The transformed *E. coli* cells were cultured (in 2-liter batches), collected 11 hours after induction, and washed with 100 ml of buffer containing 50 m*M* tris-HCl at *p*H 7.5 and 25 percent sucrose. The cells were resuspended in the same buffer with 0.01 percent NP-40 and 5 m*M* $MgCl_2$ in the presence of deoxyribonuclease. The clear lysate obtained by centrifugation at 15,000 rpm was diluted with a buffer containing 50 m*M* Hepes (sodium salts) (*p*H 7.5), 1 m*M* EDTA, 1 m*M* dithiothreitol (DTT), and 0.01 percent *n*-octyl glucoside, fractionated by DEAE Sephacel column chromatography, and further purified by Sephadex G-75 column chromatography. The overall yield was approximately 15 mg of pure proteins from a 2-liter culture. The purified proteins had one bound GDP per p21 molecule and the same NH_2-terminal sequence of Met-Thr-Glu-Tyr-Lys as the sequence predicted from the complementary DNA (cDNA) clones (*39–42*). As detected by complex formation with tritium-labeled GDP, "catalytic domains" of normal p21 (Gly^{12}, 1–171) and activated p21 (Val^{12}, 1–171), as well as full-length p21 proteins, bind GDP. The GTPase activity of p21 (Gly^{12}, 1–171) was found to be the same as that of normal p21, whereas in p21 (Val^{12}, 1–171) and p21 (Val^{12}, 1–189) it was, as predicted, less than 10 percent of normal.

We obtained good quality single crystals by the sitting drop technique from solutions containing protein (10 mg/ml), 0.1*M* $CaCl_2$, 0.075*M* Hepes (*p*H 7.5), 0.5 m*M* EDTA, 0.5 m*M* DTT, and 0.005 percent *n*-octyl glucoside equilibrated to 30 percent PEG 400. Hexagonal bipyramidal crystals with well-defined faces formed after about a week and were allowed to grow for an additional 2 to 3 weeks before the x-ray analysis. The space group of the "catalytic

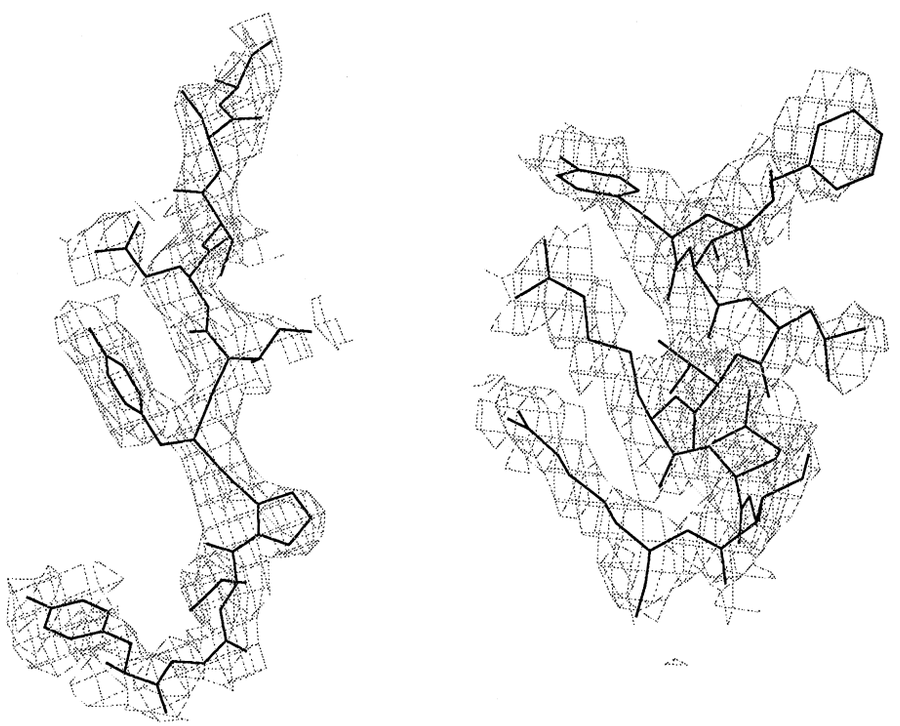

Fig. 1. Portions of the 2.7 Å electron density map superimposed with an α helical region (residues 156 to 164; Phe-Tyr-Thr-Leu-Val-Arg-Glu-Ile-Arg) at right, and a loop β strand region (residues 137 to 146; Tyr-Gly-Ile-Pro-Tyr-Ile-Glu-Thr-Ser-Ala) at left, of c-H-*ras* p21 crystal structure.

domain" crystals is $P6_522$ with cell parameters $a = b = 83.2$ Å and $c = 105.1$ Å. There is one p21 "catalytic domain" per asymmetric unit and 46 percent of the unit cell volume is protein.

Diffraction data collection and structure determination. We collected diffraction data for the native as well as five heavy-atom derivatives on x-ray films; we used an Enraf-Nonius rotation camera installed on the eight-pole wiggler branch line (Stanford Synchrotron Radiation Laboratory). The x-ray wavelength for the data collection was either 1.5418 or 1.08 Å, and the crystal-to-film distance was 60 or 85 mm. All the data were collected at 4°C. The films were digitized with the use of a drum scanner (Optronix Corp.), and the data were processed with the use of computer programs originally written by Rossmann (*43*). Reflection data from different films were merged together with the use of the PROTEIN program package (*44*). The native data set contained about 46,000 observations of 10,400 unique reflections, with an $R_{merge}(I)$ of 8 percent and a maximum resolution of 2.25 Å (Table 1). About 300 reflections, missing from this data set because of intensity overload or positional overlap on the films, were later measured with a Nicolet P3/F four-circle diffractometer and added to the native data set.

Five heavy-atom derivatives were used for phasing: three of them were obtained by soaking the crystals in solutions containing $KAuI_4$, K_2HgI_4, and K_2PtBr_6 separately, the fourth by soaking in solutions of $KAuI_4$ then K_2HgI_4 (Au/Hg), and the fifth by soaking in solutions of $KAuI_4$ then K_2PtBr_6 (Au/Pt) (Table 1). Difference Patterson maps for each derivative were calculated from diffraction data between 10 and 4 Å resolution, and interpreted for heavy-atom positions with the use of the program HASSP (*45*). For both the gold and the mercury derivative, two sites (A and B) appeared initially as two separate single-site solutions, without the cross-vector solution between them (Table 2). One single site, C, came up for the platinum derivative. The origin correlation between sites A and B was determined from the Au and Hg double-soak difference Patterson map, while that between sites A, B, and C was obtained by difference Fourier syntheses.

The multiple isomorphous replacement (MIR) refinement was initiated in space group $P6_122$ with the computer program package PROTEIN (*44*) for the three major sites (A, B, and C in Table 2), and with reflections between 40.0 and 3.0 Å resolution. The root-mean-square (rms) lack-of-closure errors were calculated from centric reflections and updated after each refinement cycle. Reflections with lack-of-closure errors greater than 2.1 times the rms value were rejected from the phase refinement. Several minor heavy-atom sites were located from difference Fourier maps and included in the refinement process (Tables 2 and 3).

We applied a noise-filtering procedure (*46*) to improve the MIR phases. The calculated electron density map showed a six-stranded β sheet and three α helices. A GDP molecule could also be seen in the map. The handedness of the α helices indicated the space group to be $P6_522$ rather than $P6_122$. Although the secondary structure could be seen in the map, the connectivity between the secondary structure elements was difficult to determine. Therefore, phasing was extended to 2.7 Å resolution (*46*). The phase extension process (Table 4) resulted in a map that helped us resolve some ambiguous regions in the original map and revealed a fourth short α helix. At this point, a partial backbone model represented by polyalanine was fit into the electron density map with the program package FRODO

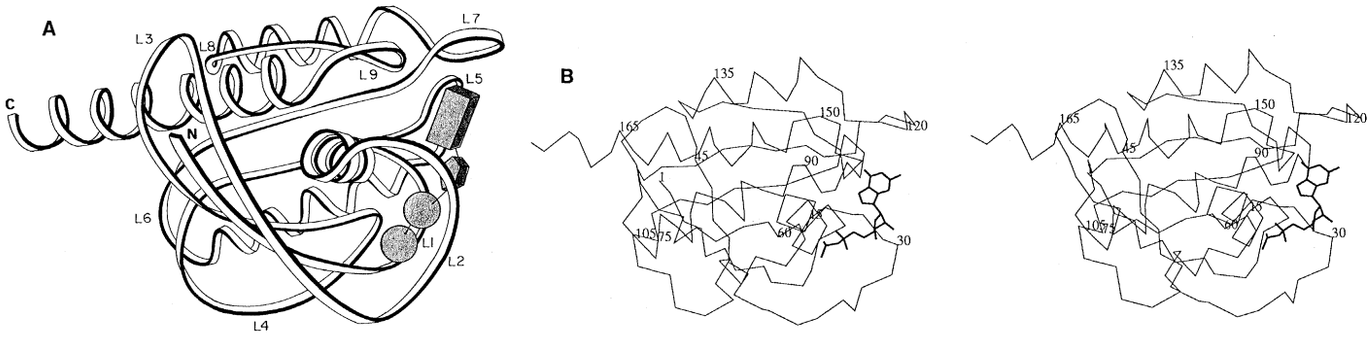

Fig. 2. (**A**). The backbone structure of the catalytic domain of human normal c-H-*ras* p21 protein. The flow of the backbone is represented by a continuous flat ribbon. The β strands can be recognized by straight runs; and the α helices by helical coils. The guanine base, the ribose, and the phosphates are represented as stippled rectangular block, pentagonal block, and spheres, respectively. The NH_2- and COOH-termini are indicated. The looped regions are numbered 1 to 9 from the NH_2-terminus. (**B**). Stereo-drawing of the α-carbon backbone structure of human normal c-H-*ras* p21.

Table 1. Heavy atom derivatives of normal human c-H-*ras* p21 crystals.

Item	Native	$KAuI_4$	K_2HgI_4	K_2PtBr_6	Au and Hg	Au and Pt
Heavy atoms (m*M*)		Sat.	2	7	Sat./2	Sat./7
Soaking (hours)		24	15	10	18/2	18/6
a (Å)	83.2	83.2	83.8	83.3	83.5	83.6
c (Å)	105.1	105.0	105.2	105.5	104.5	105.3
Resolution (Å)	2.25	2.7	2.8	3.5	2.9	3.5
Film sets (No.)	32	48	32	64	32	32
Observations (No.)	45,942	48,525	38,067	16,314	35,297	20,807
Unique reflections (No.)	10,379	5,594	4,966	2,820	4,294	2,926
R_{merge}* (%)	8.0	10.5	9.2	9.1	9.2	8.7
R_{scale}† (%)		12	16	18	23	21

*$R_{merge} = \sum_{hkl} \sum_i |\bar{I} - I_i| / \sum_{hkl} \sum_i I_i$ †$R_{scale} = \sum_{hkl} |F_P - F_{PH}| / \sum_{hkl} F_P$, where F_P and F_{PH} are the native and derivative structure factor amplitudes, respectively.

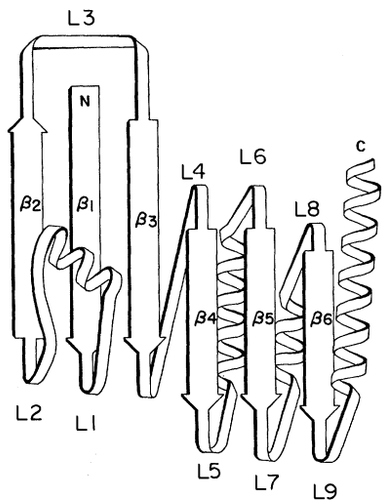

Fig. 3. Topological structure of the catalytic domain of human c-H-*ras* p21 protein. The β strands, α helices, and loops are represented as wide arrowed ribbons, helical ribbons, and narrow ribbons, respectively. Loops are numbered sequentially from NH_2- to COOH-terminus.

(*47*) for an E&S PS300 computer graphics system. Phases calculated from the partial model were combined with the original MIR phases, and improved by the noise-filtering technique (*46*). The new map helped in the assignment of side chains and a complete tracing was achieved. At this point, most of the side chains could be identified, thus confirming the correctness of the chain tracing (Fig. 1). This tracing was further supported by the location of the major heavy atom positions: site A was found to lie between Cys^{80} and Met^{111}, site B near Cys^{118}, and site C between Met^{67} and Met^{72}. The *R* factor is 26 percent at the current state of refinement.

Backbone structure and GDP-binding site. An overall view of the three-dimensional backbone structure of p21 is shown in Fig. 2 and the topological arrangement of the secondary structure elements is schematically represented in Fig. 3. The structure contains a six-stranded β sheet, four α helices, and nine connecting loops. The β sheet has the topology β2, β1, β3, β4, β5, and β6 (each β strand is numbered consecutively from NH_2- to COOH-terminus), with β2 antiparallel to the other five strands. The β sheet consists of two smaller sheets: one composed of the first three β strands (β2, β1, and β3) and the other of the remaining three strands (β4, β5, and β6) with a short stretch of hydrogen bonding between β3 and β4. Two α helices (α2 and α3) pack against the convex face of the β sheet and the remaining two (α1 and α4) pack against the concave face. Helix α2 is actually constituted by two segments and is approximately parallel to α3 and α4, whereas the axis of helix α1 is almost at right angles to the axes of the other three. The COOH-terminal helix α4 is the longest in the molecule, containing approximately seven turns, the last two turns of which form a protrusion from the otherwise globular shape of the protein. The β–α–β–α–β structure at the COOH-terminal half of the protein is similar in topology to the nucleotide-binding domain motif (*48*). Five out of nine loops are on the side of molecule where GDP is bound and the remaining four are on the opposite side. The overall dimension of the molecule is 35 by 40 by 49 Å.

The GDP molecule is bound in a pocket formed by four loops (L1, L2, L7, and L9) in the structure. Specifically, residues 10 to 16 of loop L1 are near the phosphates, and residue 30 of loop L2 is near the ribose sugar. Residues 116, 117, 119, and 120 of loop L7 and residues 145 to 147 of loop L9 form a side of the pocket for the guanine base. These four regions in the crystal structure are indicated in Fig. 4. In addition, the phenyl side chain of Phe^{28} is almost perpendicular to the guanine base—one of two common types of interaction between aromatic groups in crystals of bases (*49*) and proteins (*50*).

Almost all the known activating in vivo and in vitro point mutations (at positions 12, 13, 15, 16, 59, 61, 63, 116, and 119; for a review, see *8*) are localized within three loops L1, L4, and L7: residues 12, 13, 15, and 16 in loop L1 are near the phosphates, therefore mutations at these positions may directly affect the GDP or GTP binding and the hydrolysis of GTP (see below). Similarly, mutations at residues 116 and 119 in loop L7 may have direct influence on the guanine base binding. Residues 59, 61, and 63 belong to loop L4, which is not in contact with the phosphate groups of GDP but in direct contact with loop L1. It seems possible that mutations at these positions in loop L4 may activate p21 through indirect conformational changes of loop L1. Furthermore, their positions in the structure are in the pocket that the γ phosphate would have occupied in the GTP-bound form, thus mutation in those positions may in addition affect GTP binding or GTPase activity. There are several other residues lining the GDP-binding pocket. The details of the interaction of guanine nucleotides with these and other residues are expected to be revealed when the structure refinement at 2.25 Å resolution is completed.

Active site for GTPase function and phosphate acceptor. Loop L1 is very unusual in its amino acid composition, that is, rich in small residues. The amino acid sequence of this loop is Gly-Ala-Gly-Gly-Val-Gly. This loop is located just below the β phosphate of GDP, and would have straddled the phosphoester bond between the β and γ phosphate of GTP (see Fig. 4). The location of the loop in relation to the phosphate group of GDP makes it the prime candidate for the GTPase catalytic site. Its highly constrained conformation also explains the critical nature of the residues in this loop; for example, substitution at residue 12 by any amino acid other than Gly or Pro endows the protein with transforming activity (*51*).

Viral p21 proteins have a phosphorylated threonine at residue 59. This residue is located at the COOH-end of the β3 strand, adjacent to the phosphate-binding loop L1. If we imagine the γ phosphate of GTP extending out from the β phosphate into the GDP-binding pocket, the likely direction it will take appears to be toward the end of the β3 strand, where Thr^{59} of viral protein would be located to receive, with a minor conformational change, the γ phosphate group. This also suggests that loop L1 contains the catalytic residues responsible for hydrolysis of GTP resulting in autophosphorylation of Thr^{59}.

Table 2. Heavy atom positions in normal human c-H-*ras* p21 crystals.

Compound	Heavy atom positions*			Occupancy	Temp. factor	Site
	x	*y*	*z*			
$KAuI_4$	0.4741	0.2112	0.2417	26	30	A
	0.3545	0.0570	0.4125	17	41	B
	0.8120	0.4692	0.0371	10	40	
K_2HgI_4	0.4816	0.1972	0.2446	34	42	A
	0.3589	0.0424	0.4120	26	50	B
	0.0860	0.8881	0.0531	11	36	
K_2PtBr_6	0.6561	0.1559	0.5753	35	36	C
	0.1722	0.0486	0.0409	19	32	
	0.8097	0.4716	0.0361	14	35	
	0.3831	0.1751	0.0375	11	36	
	0.4180	0.3884	0.0444	9	31	
Au/Hg	0.4733	0.2097	0.2412	50	21	A
	0.3551	0.0573	0.4134	42	41	B
Au/Pt	0.6589	0.1562	0.5765	64	54	C
	0.1739	0.0506	0.0392	25	24	
	0.3991	0.2725	0.0176	7	45	

*These are fractional coordinates of the heavy atoms in space group $P6_122$; (x, y, ½ − z) will give the positions in space group $P6_522$.

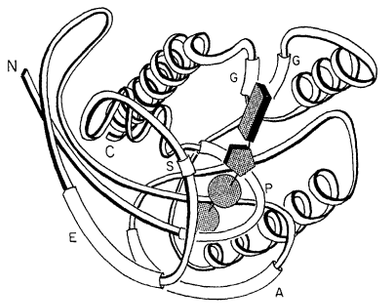

Fig. 4. The backbone structure of human normal c-H-*ras* p21 protein looking into the GDP-binding pocket. The viewing direction is rotated 90° around a vertical axis from that of Fig. 2. The regions that bind guanine base (G), ribose sugar (S), phosphates (P), and neutralizing antibody Y13-259 (A), as well as the "effector" region (E) are indicated by sleeved tubes.

Table 4. Statistics of phase extension.

	Initial data	Phase extended data
Resolution (Å)	3.0	2.7
Reflections (No.)	4123	2022
Figure of merit	0.83	0.74
R factor*	0.29	0.30
Average Δϕ†	29.7	
Root-mean-square Δϕ	50.6	

*$R^2 = \sum(F_{obs} - F_{cal})^2/\sum F_{obs}^2$. †Δϕ, accumulated phase difference.

Epitope for neutralizing antibody and "effector" region. A monoclonal antibody, Y13-259 (*52*), has been shown to inhibit morphological transformation induced by activated *ras* proteins (*53, 54*). The antibody recognition site includes six of the side chains of the region 63–73 (*55*). This entire region is a part of loop L4 (Fig. 4), almost opposite to the GDP-binding site. A tentative explanation for the neutralizing effect may be that the antibody binding induces a conformational change in loop L4, which in turn affects loop L1 due to their direct contacts; this may revert the active site (loop L1) conformation from a transforming to a normal state. This region may be a good target for drug design to alter the conformation of loop L4 in a similar way.

Amino acid substitutions in the region between residues 35 and 40 reduce the transformation capacity of activated *ras* proteins without affecting their GTPase activity or guanine nucleotide binding (*55*). This suggests that these regions are involved in the effector activity of *ras* proteins, for example, in the interaction of *ras* proteins with their putative cellular target proteins. The three-dimensional structure shows that this region belongs to the COOH-terminal end of loop L2 and the beginning of the following β strand (Fig. 4). This part of the molecule is not in direct contact with (but near) the GDP, located on the outside, and very well exposed. There are several other regions just as exposed as this, and they could be good candidates as effector regions.

Comparisons. Amino acid sequences of several GDP-binding proteins revealed that, although the sequence similarity is limited, there are four separate regions of sequence similarity between them and p21 proteins, if conservative substitutions are permitted (*56*). Since the crystal structure of one of them, the GDP-binding domain of EF-Tu, has been determined (*57, 58*), attempts have been made to predict the three-dimensional structure of p21 (*57, 59*). The predicted models have overall similarity to the p21 crystal structure in that both have a six-stranded β sheet with α helices on both sides of the sheet. On closer examination, the models are similar to the crystal structure for the region between residues 1 and 25, which corresponds to the first NH_2-terminal β strand, loop L1, and helix α1, then differ substantially until residue 78. The nucleotide-binding motif, spanning residues 78 to 142, is similar in overall topology but differs in detail between the models and the crystal structure.

Neoplasia by the *ras* gene family has been observed to occur by at least three different mechanisms: infection by a retrovirus bearing *ras* oncogenes, carcinogen-induced mutation of a cellular *ras* proto-oncogene to oncogene, and insertional mutation at the regulatory element of cellular *ras* proto-oncogenes (*8*). The former two processes produce activated p21 proteins, and the third results in an abnormal amount of normal p21 proteins, thus presumably disrupting the proper regulation of signal transduction by p21 proteins to target proteins. The possible role of p21 proteins as G proteins invites speculation that p21 might have surface regions specific to one or more target proteins and other regions specific to one or more signal receptor molecules, and that signal transduction may be mediated by a conformational change of p21 proteins. The crystal structure reveals that nine looped regions are exposed at the surface of the protein, of which four are used for GDP or GTP binding and GTP hydrolysis. Indeed, one or some of the remaining loops as well as exposed α helices may be important for recognition by particular target proteins and signal receptor molecules.

Table 3. Statistics of MIR refinement of normal human c-H-*ras* p21.

Resolution (Å)	19.8	11.0	7.62	5.82	4.71	3.96	3.41	3.00	Total
Native									
Figure of merit	0.94	0.91	0.81	0.85	0.84	0.72	0.66	0.61	0.70
Reflections (No.)	11	63	170	344	539	764	1057	1333	4281
$KAuI_4$									
Phasing power*	0.80	1.94	1.62	2.14	2.13	1.44	1.43	1.07	1.57
R_{Cullis}†	0.59	0.44	0.54	0.46	0.47	0.57	0.59	0.67	0.55
K_2HgI_4									
Phasing power	1.20	1.28	1.60	2.52	1.30	1.16	1.16	1.47	1.46
R_{Cullis}	0.53	0.68	0.46	0.32	0.65	0.61	0.62	0.60	0.56
K_2PtBr_6									
Phasing power	3.48	2.85	1.44	1.43	1.76	1.30	1.27		1.69
R_{Cullis}	0.49	0.38	0.51	0.59	0.50	0.63	0.59		0.56
Au/Hg									
Phasing power	1.92	2.00	1.92	2.84	2.81	1.86	1.57	1.56	2.06
R_{Cullis}	0.29	0.44	0.47	0.33	0.33	0.51	0.51	0.54	0.45
Au/Pt									
Phasing power	0.79	1.59	1.71	1.95	1.68	1.08	1.02		1.23
R_{Cullis}	0.65	0.54	0.57	0.45	0.55	0.67	0.67		0.59

*Phasing power = $\sqrt{\sum f_H^2/\sum (F_{PH}^{obs} - F_{PH}^{calc})^2}$. †$R_{Cullis} = \sum|F_{PH}^{obs} - F_{PH}^{calc}|/\sum|F_{PH}^{obs} - F_P|$ (for centric reflections).

The structure of the "catalytic domain" of p21 lacks 18 residues at the COOH-terminus. The long COOH-terminal α helix in this structure suggests that the "catalytic domain" is well separated from the membrane attachment domain. This long α helix could play an important role in transmitting a signal from the membrane attachment domain [receptor recognition domain (?)] to the "catalytic domain," and in keeping the "catalytic domain" some distance away from the membrane surface.

We have recently crystallized the "catalytic domains" of two activated human c-H-*ras* p21 proteins, p21(Val^{12}) and p21(Leu^{61}). Preliminary crystallographic studies show that the space group and cell parameters are identical to those of the normal human c-H-*ras* p21 "catalytic domain," which suggests that the structural differences between the normal and activated structures of p21 proteins complexed with GDP are small, perhaps limited to the regions near residue 12 or 61 (or both). However, this does not allow us to assess the extent of possible conformational differences between GTP complexes of normal and activated p21 proteins. The α carbon coordinates will be deposited in the Brookhaven Protein Data Bank.

REFERENCES AND NOTES

1. S. Nishimura and T. Sekiya, *Biochem. J.* **243**, 313 (1987).
2. C. Shih, L. C. Padhy, M. Murray, R. A. Weinberg, *Nature (London)* **290**, 261 (1981).
3. T. G. Krontiris and G. M. Cooper, *Proc. Natl. Acad. Sci. U.S.A.* **78**, 1181 (1981).
4. M. Perucho *et al.*, *Cell* **27**, 467 (1981).
5. S. Pulciani *et al.*, *Proc. Natl. Acad. Sci. U.S.A.* **79**, 2845 (1982).
6. J. J. Harvey, *Nature (London)* **204**, 1104 (1964).
7. W. H. Kirsten and L. A. Mayer, *J. Natl. Cancer Inst.* **39**, 311 (1967).
8. M. Barbacid, *Annu. Rev. Biochem.* **56**, 779 (1987).
9. C. J. Tabin *et al.*, *Nature (London)* **300**, 143 (1982).
10. E. P. Reddy, R. K. Reynolds, E. Santos, M. Barbacid, *ibid.*, p. 149.
11. E. Taparowsky *et al.*, *ibid.*, p. 762.
12. C. J. Quaife, C. A. Pinkert, D. M. Ornitz, R. D. Palmiter, R. L. Brinster, *Cell* **48**, 1023 (1987).
13. A. G. Gilman, *Annu. Rev. Biochem.* **56**, 615 (1987).
14. E. M. Scolnick, A. G. Papageorge, T. Y. Shih, *Proc. Natl. Acad. Sci. U.S.A.* **76**, 5355 (1979).
15. T. Y. Shih, A. G. Papageorge, P. E. Stokes, M. O. Weeks, E. M. Scolnick, *Nature (London)* **287**, 686 (1980).
16. F. Tamanoi, M. Walsh, T. Kataoka, M. Wigler, *Proc. Natl. Acad. Sci. U.S.A.* **81**, 6924 (1984).
17. G. L. Temeles, J. B. Gibbs, J. S. D'Alonzo, I. S. Sigal, E. M. Scolnick, *Nature (London)* **313**, 700 (1985).
18. J. B. Gibbs, I. S. Sigal, M. Poe, E. M. Scolnick, *Proc. Natl. Acad. Sci. U.S.A.* **81**, 5704 (1984).
19. J. P. McGrath, D. J. Capon, D. V. Goeddel, A. D. Levinson, *Nature (London)* **310**, 644 (1984).
20. R. W. Sweet *et al.*, *ibid.* **311**, 273 (1984).
21. V. Manne, E. Bekesi, H. F. Kung, *Proc. Natl. Acad. Sci. U.S.A.* **82**, 376 (1985).
22. T. Y. Shih, P. E. Stokes, G. W. Smythers, R. Dhar, S. Oroszlan, *J. Biol. Chem.* **257**, 11767 (1982).
23. A. Fujiyama and F. Tamanoi, *Proc. Natl. Acad. Sci. U.S.A.* **83**, 1266 (1986).
24. B. M. Sefton, I. S. Trowbridge, J. A. Cooper, E. M. Scolnick, *Cell* **31**, 465 (1982).
25. Z. Q. Chen, L. S. Ulsh, G. DuBois, T. Y. Shih, *J. Virol.* **56**, 607 (1985).
26. J. E. Buss and B. M. Sefton, *Mol. Cell. Biol.* **6**, 116 (1986).
27. M. C. Willingham, I. Pastan, T. Y. Shih, E. M. Scolnick, *Cell* **19**, 1005 (1980).
28. B. M. Willumsen, A. Christensen, N. L. Hubbert, A. G. Papageorge, D. R. Lowy, *Nature (London)* **310**, 583 (1984).
29. K. Shimizu *et al.*, *ibid.* **304**, 497 (1983).
30. E. Taparowsky, K. Shimizu, M. Goldfarb, M. Wigler, *Cell* **34** 581 (1983).
31. B. M. Willumsen *et al.*, *EMBO J.* **4**, 2893 (1985).
32. B. M. Willumsen, K. Norris, A. G. Papageorge, N. L. Hubbert, D. R. Lowy, *ibid.* **3**, 2581 (1984).
33. J. B. Hurley, M. I. Simon, D. B. Teplow, J. D. Robishaw, A. G. Gilman, *Science* **226**, 860 (1984).
34. T. Tanabe *et al.*, *Nature (London)* **315**, 242 (1985).
35. M. A. Lochrie, J. B. Hurley, M. I. Simon, *Science* **228**, 96 (1985).
36. H. Itoh *et al.*, *Proc. Natl. Acad. Sci. U.S.A.* **83**, 3776 (1986).
37. J. Jancarik *et al.*, *J. Mol. Biol.*, in press.
38. K. Miura *et al.*, *Jpn. J. Canc. Res. (Gann)* **77**, 45 (1986).
39. S. Pulciani *et al.*, *Proc. Natl. Acad. Sci. U.S.A.* **79**, 2845 (1982).
40. M. Goldfarb, K. Shimizu, M. Perucho, M. Wigler, *Nature (London)* **296**, 404 (1982); C. Shih and R. A. Weinberg, *Cell* **29**, 161 (1982).
41. D. J. Capon, E. Y. Chen, A. D. Levinson, P. H. Seeburg, D. V. Goeddel, *Nature (London)* **302**, 33 (1983).
42. E. P. Reddy, *Science* **220**, 1061 (1983).
43. M. G. Rossmann, *J. Appl. Cryst.* **12**, 225 (1979).
44. W. Steigemann, *PROTEIN: A Package of Crystallographic Programs for Analysis of Proteins* (Max Planck Institute for Biochemistry, Martinsried, West Germany, 1982).
45. T. Terwilliger, S.-H. Kim, D. Eisenberg, *Acta Cryst.* **A43**, 1 (1987).
46. B. C. Wang, *Methods Enzymol.* **115**, 90 (1985).
47. A. Jones, *FRODO: A Molecular Graphics Program*, University of Uppsala, Uppsala, Sweden; subsequently modified by B. L. Bush at Merck, Sharp & Dohme, Rahway, NJ, and by J. W. Pflugrath, M. A. Saper, J. S. Sack, Rice University, Houston, TX.
48. S. T. Rao and M. G. Rossmann, *J. Mol. Biol.* **76**, 241 (1973).
49. S.-H. Kim and A. Rich, *ibid.* **42**, 87 (1969).
50. S. K. Burley and G. A. Petsko, *Science* **229**, 23 (1985).
51. P. H. Seeburg, W. W. Colby, D. J. Capon, D. V. Goeddel, A. D. Levinson, *Nature (London)* **312**, 71 (1984).
52. M. E. Furth, L. J. Davis, B. Fleurdelys, E. M. Scolnick, *J. Virol.* **43**, 294 (1982).
53. L. S. Mulkahy, M. R. Smith, D. W. Stacey, *Nature (London)* **313**, 241 (1985).
54. H. F. Kung, M. R. Smith, E. Bekesi, V. Manne, D. W. Stacey, *Exp. Cell Res.* **162**, 363 (1986).
55. I. S. Sigal, J. B. Gibbs, J. S. D'Alonzo, E. M. Scolnick, *Proc. Natl. Acad. Sci. U.S.A.* **83**, 4725 (1986); B. Willumsen *et al.*, *Mol. Cell. Biol.* **6**, 2646 (1986).
56. R. Leberman and U. Egner, *EMBO J.* **3**, 339 (1984).
57. F. Jurnak, *Science* **230**, 32 (1985).
58. T. F. M. la Cour, J. Nyborg, S. Thirup, B. F. C. Clark, *EMBO J.* **4**, 2385 (1985).
59. F. McCormick *et al.*, *Science* **230**, 78 (1985).

60. We thank P. Phizackerley, Stanford Synchrotron Radiation Laboratory, Palo Alto, CA, for help in data collection. Supported in part by grants from NIH (GM 29287 and CA 45593) and DOE (S.H.K.); a gift from Merck, Sharp & Dohme to the University of California, Berkeley; grants-in-aid from the Japanese Ministry of Health and Welfare for a comprehensive 10-year strategy for cancer control (Su.N.); a research resident fellowship from the Foundation for Promotion of Cancer Research (Tokyo) (Sh.N.); and a Damon Runyon–Walter Winchell Cancer Fellowship (P.M.M.).

30 October 1987; accepted 22 December 1987